Interaction of ^{154}Gd nuclei with their environment in a Cu matrix

M. B. Kurup, K. G. Prasad, and R. P. Sharma
Tata Institute of Fundamental Research, Bombay, India
(Received 13 May 1975)

Time integral and differential perturbed angular correlation measurements have been carried out on ^{154}Gd using implanted samples of ^{153}Eu in Cu which are irradiated with neutrons to produce radioactive ^{154}Eu $\xrightarrow{\beta^-}$ ^{154}Gd ($\tau_{1/2} \sim 15$ yr). The integral attenuation factors $\bar{G}_{22}(\infty)$ and $\bar{G}_{44}(\infty)$ so obtained from a study of the 1278–123-keV ($2^- \rightarrow 2^+ \rightarrow 0^+$) and 876–123-keV ($2^+ \rightarrow 2^+ \rightarrow 0^+$) γ-γ cascades in ^{154}Gd are 0.482 ± 0.045 and 0.69 ± 0.18, respectively. These values combined with time-differential measurements have revealed a predominantly static electric-quadrupole-interaction behavior of ^{154}Gd nuclei in a diamagnetic Cu host. The electric field gradient at the interaction site is found to be of the order of 3×10^{17} V/cm^2. Using the channeling of 2-MeV α particles in single crystals of Cu implanted with ^{153}Eu, it is found that $> 90\%$ of the impurity ions occupy nonsubstitutional sites and at the same time there is considerable radiation damage. We have not found any evidence of internal oxidation of Gd ions on annealing the implanted sample in a hydrogen atmosphere even at 500°C for 5 h. The annealed samples do not show any change in the attenuation factor $\bar{G}_{22}(\infty)$ as compared to the unannealed samples, while the same factor for an oxide sample has been found to be 0.77 ± 0.06.

I. INTRODUCTION

Several investigations[1–4] of the nuclear hyperfine interaction on rare-earth impurities implanted into magnetic and nonmagnetic metallic lattices have been carried out in recent years. These measurements have shown that the integral perturbed angular correlations (PAC) of rare earths in Fe and also in Cu are highly attenuated.[5,6] The observed attenuations have been attributed mainly to time-dependent magnetic interactions. The nature of the relaxation processes, responsible for such time dependence of the magnetic hyperfine interactions, is further studied by time-differential PAC techniques. In a number of rare earths like Nd, Sm, Dy, Er, etc., this technique has been employed[7] following Coulomb excitation and then recoil implantation in Cu backing using high-energy (20–50 MeV) heavy-ion beams. It is inferred from such measurements that the interaction in these cases is not simply a time-dependent magnetic one alone as mentioned above, but it is described much better by a combination of both magnetic and electric time-dependent interactions.

A detailed investigation of the various contributions to the hyperfine field interacting with the nuclei in a host material is very important to understand the nature of the interaction, which may be electric or magnetic, static or time dependent, or a combination of all these. Let us take the case of rare earths in a nonmagnetic host like Cu, where the dominant contribution to the magnetic hyperfine field at an impurity nucleus is due to its $4f$ electrons. Effects of the neighboring ions, conduction-electron and core polarizations, lattice damages, etc., may contribute to both magnetic as well as electric hyperfine interactions. Their magnitudes predominantly depend on the exact location of the impurity in the host material. For example, at a substitutional site in a cubic host lattice like that of Cu where the electric field gradient is almost zero, the perturbations due to the host environment will be negligible, but nonsubstitutional locations and lattice damage due to radiation may completely change this picture and strong electric field gradients could be anticipated.

It is possible to study these effects separately in suitable cases. One such case is Gd^{3+}; being an S-state ion with half-filled $4f$ shell (electronic configuration $^8S_{7/2}$) it has $L = 0$. Consequently the $4f$ field vanishes except for some small polarization effects. The spin-lattice interaction is also negligible. Thus in a Cu host, the field seen by the Gd^{3+} nuclei is mainly due to the neighboring ions, depending on its location. From the earlier time-differential PAC measurements[7] following Coulomb excitation and recoil implantation of Gd into Cu using a 25-MeV oxygen beam, it appeared that the correlation may be attenuated by an electric interaction for a few nanoseconds, and the attenuation then stops. Furthermore the relaxation time for any fluctuating field present is found to be long.

In the present work both integral and time-differential PAC techniques are employed for a detailed study of the interaction of $^{154}Gd^{3+}$ nuclei with their environment using the radioactive decay of ^{154}Eu $\rightarrow$ ^{154}Gd produced by neutron irradiation of ^{153}Eu ions implanted in a diamagnetic Cu host.

Recently, Cohen *et al.*[8] have reported the possibility of internal oxidation of the implanted rare-earth atoms in an iron host after annealing the

sample in hydrogen atmosphere. They find, by Mössbauer measurements, that internal oxidation is complete after annealing for about 15 min at 480 °C and consequently the hyperfine field vanishes at the rare-earth sites. In order to investigate whether such internal oxidation occurs in the sample used in the present experiment, we have carried out the integral PAC measurements after annealing under the conditions specified in Ref. 8.

Separate experiments of α-particle channelling in single crystals of Cu implanted with ^{153}Eu have been carried out to find the location of the Gd-impurity ions in the host material.

II. EXPERIMENTAL DETAILS AND MEASUREMENTS

A. Source preparation

The radioactive ^{154}Eu ($\tau_{1/2} \sim 15$ yr) sources used in the present work are of three types, viz., liquid, implanted, and oxide sources. The liquid source is in the form of $EuCl_2$ aqueous solution. The second type is prepared by implanting ^{153}Eu (energy 400 keV, dose $\sim 3\times 10^{15}$ ions/cm^2), using a mass separator, into a thin pure copper foil and irradiating it with neutrons in a flux of 10^{13} neutrons/cm^2 sec for about 30 days. The oxide source is a neutron-irradiated Eu_2O_3 powder enriched in ^{153}Eu.

For the internal-oxidation studies the implanted and irradiated samples are annealed in hydrogen atmosphere.

For channelling experiments single crystals of copper were implanted with ^{153}Eu under exactly similar conditions as those given above.

B. Experimental arrangement (integral and differential PAC)

The source is mounted on the cold finger of a specially made Dewar placed on an adjustable stand with the freedom of $x-y$ movement in the horizontal plane for accurate centering of the source (better than 1%). The temperature of the sample in this Dewar could be varied from 80 °K to 300 °K.

The integral PAC measurements are carried out with two $\gamma-\gamma$ cascades, 1278–123 keV ($2^- \to 2^+ \to 0^+$) and 876–123 keV ($2^+ \to 2^+ \to 0^+$) in ^{154}Gd (Fig. 1), using both implanted and liquid sources, respectively. The 123-keV transition in the former cascade is detected in a 20-cm^3 Ge(Li) detector kept at a fixed angle, while the other γ ray is detected in a 2.54-cm $\times$ 3.8-cm-diam NaI(Tl) scintillator. In the other case, to avoid the interference of the neighboring γ transitions feeding the 123-keV level, the Ge(Li) detector is used for the 876-keV transition while the NaI(Tl) scintillator for the 123-keV γ ray. A conventional fast-slow coincidence arrangement with resolving time 0.1 μsec has been used in these measurements and the coincidence spectra in the 123-keV region are recorded in a multichannel analyzer at four angles (180°, 150°, 120°, and 90°). All corrections arising due to the background from the γ transitions other than those of the cascade under consideration, backscattering, etc., have been suitably taken into account.

1. 1278-123-keV cascade

The multichannel spectra (Fig. 2) at all angles in this case have clearly shown the 248-keV photopeak well separated from the backscattered peaks. From the intensity of the 248-keV transition, the contribution of the background in the 123-keV region due to partial acceptance of 1249-keV γ rays in the gate has been accurately determined at each angle. Transitions above 1278 keV are weak in intensity, and the correction due to their Compton contribution is taken into account by shifting the gate adjacent to the higher side of the 1278-keV photopeak and then recording the coincidence spectra under identical conditions as mentioned above.

The analysis of the coincidence spectrum at each angle is carried out in the usual way taking into account various contributions including the corrections of chance coincidences and the angular distribution function $W(\theta)$ normalized to $W(\pi/2)$ is obtained as shown in Fig. 3. A least-

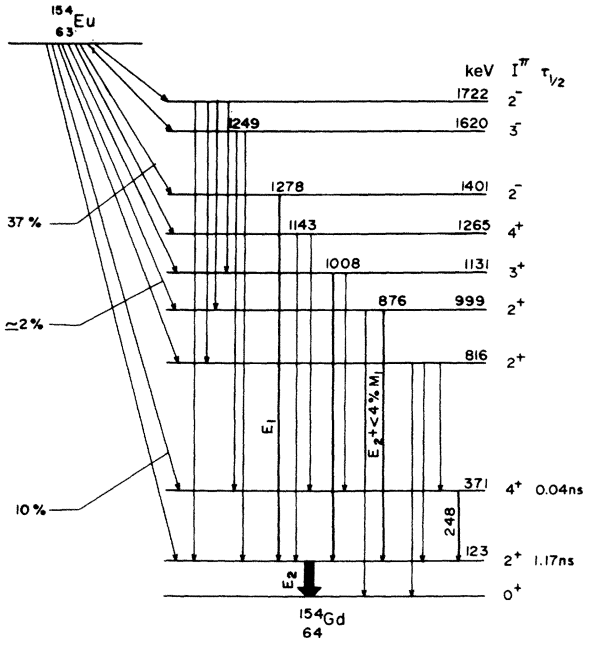

FIG. 1. Relevant part of the decay scheme of ^{154}Eu $\to$ ^{154}Gd, indicating the transitions of interest in the present work.

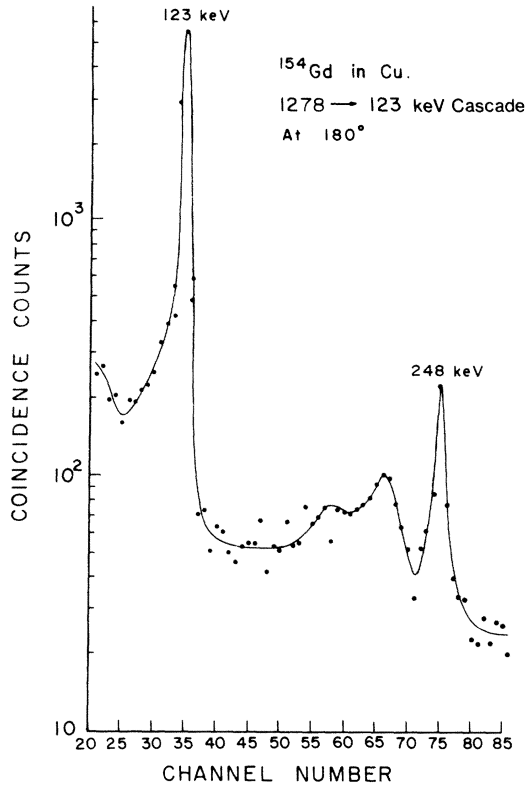

FIG. 2. γ-ray spectrum in the region of 123 keV, as recorded with a 20-cc Ge(Li) detector, in coincidence with the 1278-keV photopeak. In this spectrum the 248-keV γ ray is well resolved from the backscattered region.

square fit of the theoretical function

$$W(\theta) = 1 + A_{22}G_{22}P_2\cos\theta + A_{44}G_{44}P_4\cos\theta$$

to the experimental points in Fig. (3) is made for the implanted source. The attenuated integral angular correlation coefficients $A_{22}G_{22}$ and $A_{44}G_{44}$ corrected for detector geometry are found at two temperatures (80 °K and 300 °K) (Table I). By comparing these coefficients with the unattenuated ones (as seen in the liquid source) the value of $\bar{G}_{22}(\infty)$ for the 123-keV state is obtained. Proper analysis of the observed angular distribution of this cascade in the liquid source yields an $A_{22} = 0.226 \pm 0.005$ for the 123-keV level in ^{154}Gd. This value agrees with the theoretically calculated unattenuated A_{22} coefficient for the $2^- \to 2^+ \to 0^+$ cascade within experimental errors, and is in conformity with the quoted result of Varnell *et al.*[9] The coefficient A_{44} for this $2^- \to 2^+ \to 0^+$ cascade is almost zero.

2. 876–123-keV ($2^+ \to 2^+ \to 0^+$) cascade

The coincidence spectrum of the 123-keV γ ray in this cascade, scanned in the NaI(Tl) scintillator has all the features of the one observed above in the case of the 1278–123-keV cascade, except that the energy resolution is not good enough to clearly resolve the backscattered and the 248-keV peaks. However, these have been taken into account by stripping the spectrum using standard line shapes. The observed spectrum is also corrected for the Compton background coincidence events as described earlier in the 1278–123-keV case by setting the window beyond the 876-keV photopeak.

From the analysis of the observed data, carried out analogously as before, the $A_{22}G_{22}$ and $A_{44}G_{44}$ values corrected for detector geometry are obtained (Table I). The integral attenuation factor $\bar{G}_{44}(\infty)$ is calculated by comparing the observed result with the unattenuated one as seen in the liquid source. (The coefficient A_{22} for this cascade is very small.)

3. Time-differential measurement

The differential PAC measurements on a 1278–123-keV cascade are carried out using a standard ORTEC TAC set up. In this case a lead-loaded plastic scintillator has been used on the low-energy side to improve the time resolution (full width at half-maximum 1.5 nsec). The time spectra are alternately scanned for 40 min each time in the multichannel analyzer at 90° and 180°, respectively. These measurements are carried out over a period of 10 days to improve the statistics. From an analysis of the time spectra at the two angles the time-differential attenuation coefficient $G_{22}(t)$ is obtained as shown in Fig. 4.

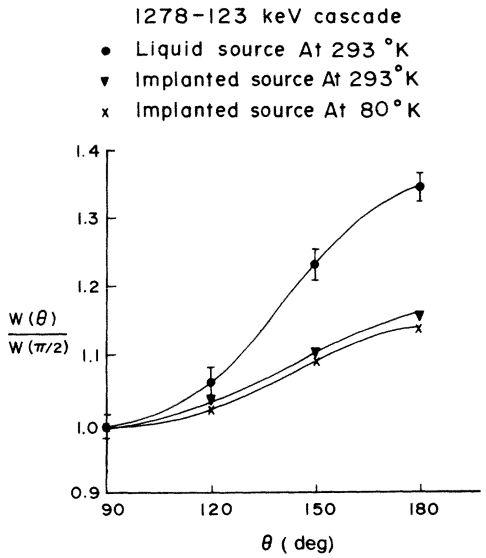

FIG. 3. Time integrated PAC measurements for the 1278–123-keV γ-γ cascade in ^{154}Gd, showing the plots of $W(\theta)/W(\frac{1}{2}\pi)$ vs θ for the liquid and implanted samples. The errors on the experimental points are the same in all cases. The solid lines are the least-square fits to the experimental points.

TABLE I. Time-integral attenuation coefficients for the γ-γ directional correlations in ^{154}Gd, observed using ^{154}Eu samples in different forms.

Cascade (keV)	Nature of the ^{154}Eu sources	Temperature (°K)	$A_{22}G_{22}$	$A_{44}G_{44}$	$\bar{G}_{22}(\infty)$	$\bar{G}_{44}(\infty)$
1278–123	$EuCl_2$ aqueous solution	293	0.226 ± 0.005	0.016 ± 0.011	...	...
1278–123	Implanted in Cu	293	0.109 ± 0.010	0.014 ± 0.019	0.482 ± 0.045	...
1278–123	Implanted in Cu	82	0.100 ± 0.011	0.018 ± 0.022	0.443 ± 0.049	...
876–123	$EuCl_2$ aqueous solution	293	−0.008 ± 0.016	0.271 ± 0.035	...	...
876–123	Implanted in Cu	293	−0.025 ± 0.023	0.188 ± 0.042	...	0.69 ± 0.18
1278–123	Eu_2O_3 powder	293	0.175 ± 0.014	0.015 ± 0.023	0.77 ± 0.06	...
1278–123	Implanted in Cu and annealed at 500 °C for 5 h in H_2 atmosphere	293	0.102 ± 0.012	0.012 ± 0.021	0.451 ± 0.054	...

C. Measurements with annealed samples

The implanted sample of ^{154}Eu has been annealed at 325 °C for 15 min in hydrogen atmosphere. The temperature is increased slowly and after annealing for the required time it is gradually decreased to room temperature. The directional distribution of the 1278–123-keV cascade is studied with this annealed sample, at room temperature, in an exactly similar way as described above. Next, the sample is annealed at 500 °C for 30 min and also for 5 h, and in both the cases the directional distribution measurements are repeated. The results are shown in Fig. 5, for the unannealed and the annealed (30 min at 500 °C) samples. No marked effect has been observed due to the change in annealing temperature and time.

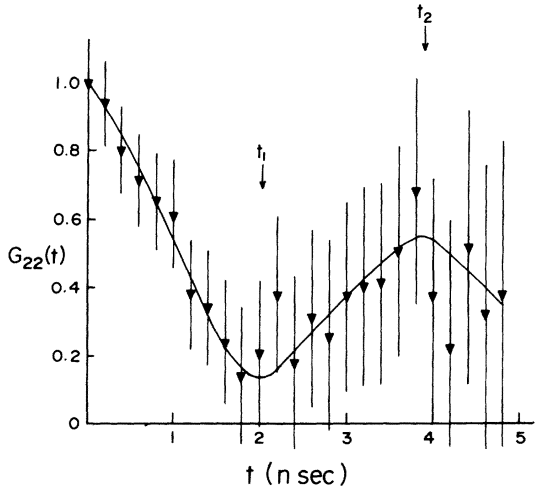

FIG. 4. Time-differential PAC measurements for the 1278–123-keV γ-γ cascade indicating the variation of $G_{22}(t)$ with time. The solid line is hand fitted. The time t_1 and t_2 are 2.1 and 3.95 nsec, respectively.

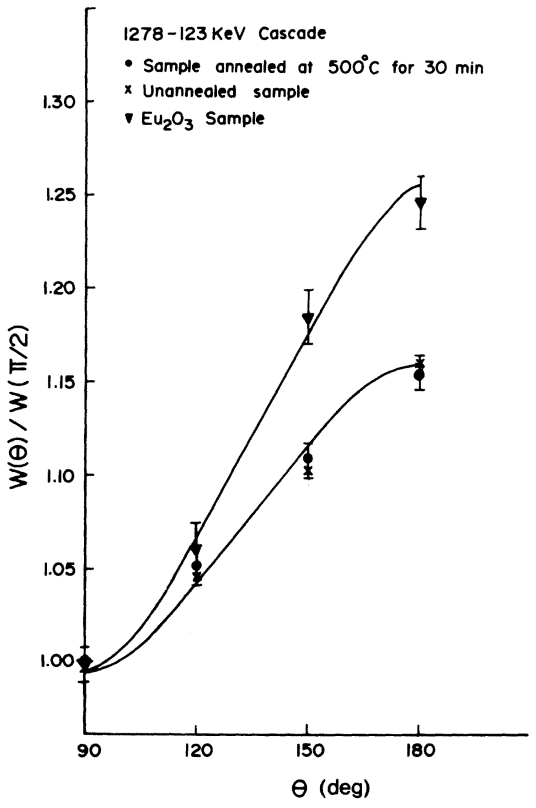

FIG. 5. Integral PAC measurements of 1278–123-keV cascade for the implanted sample before and after annealing in hydrogen atmosphere. Results of the measurements after annealing at 325 °C for 15 min and 500 °C for 5 h are almost similar to the one shown above. The correlation for an oxide sample of ^{154}Eu in the form of Eu_2O_3 is also given for comparison.

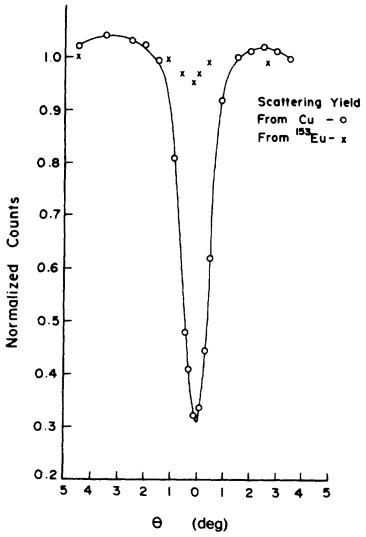

FIG. 6. Angular scan across the ⟨110⟩ axis in Eu-implanted Cu single crystal with the 2-MeV incident α particles. The scattering yields from the Cu and Eu atoms are normalized to random values.

In order to see the magnitude of the attenuation factor $\overline{G}_{22}(\infty)$ in the oxide sample, a separate measurement of the angular distribution of the 1278–123-keV cascade in the decay of a ^{154}Eu sample taken in the form of Eu_2O_3 powder has been carried out. The observed $A_{22}G_{22}$ is 0.175 ± 0.014 which corresponds to an attenuation coefficient $\overline{G}_{22}(\infty)$ equal to 0.77 ± 0.06. This value is much larger than that observed (0.482 ± 0.045) in the implanted source.

D. Channeling experiments

A well collimated (0.5 mm $\times$ 0.5 mm^2) beam of 2-MeV α particles from a 5.5-MeV Van de Graaff machine is allowed to fall on a single crystal of copper, implanted with the same energy and dose of ^{153}Eu ions as above, mounted on a double-axes goniometer. The crystal is first aligned along the ⟨110⟩ direction in the usual way by the channelling technique. To minimize the contamination of the crystal surface from oil vapor, etc., it is kept suitably surrounded by a cold trap cooled to liquid-nitrogen temperature during the measurements. The scattering yield of the α particles scattered through 150° from just below the crystal surfaces, measured as a function of the angle θ between the incident α beam and the ⟨110⟩ axis is shown in Fig. 6. A threefold dip is seen when the incident beam gets aligned with the ⟨110⟩ axis. No such reduction is observed in the scattering yield from the impurity ions. The energy spectra of these scattered α particles are also recorded in the multichannel analyzer for the incident beam in a random direction and parallel to the ⟨110⟩ axis, respectively (Fig. 7). From an analysis of these data the minimum scattering yield χ_{min} from the impurity atoms has been obtained for the incident beam aligned along the ⟨110⟩ direction of the crystal. Since the reduction in scattering yield along this direction is small (~10%), it is evident that more than 90% of the impurity atoms are not located

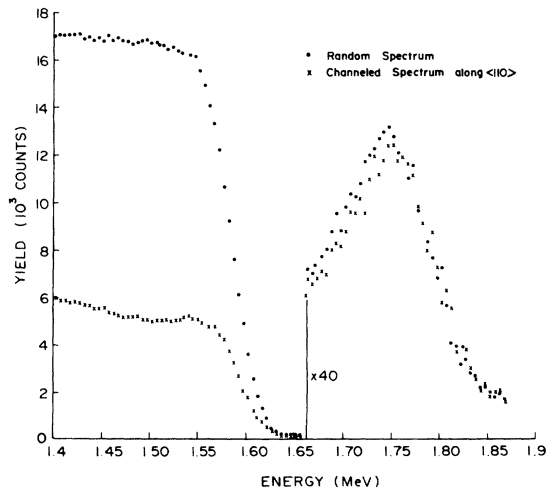

FIG. 7. Backscattered energy spectra for 2-MeV α particles incident along ⟨110⟩ and random directions, respectively, in a Cu single crystal implanted with ^{153}Eu. The vertical scale in the high-energy region has been expanded and the pile-up effects are suitably taken into account in this region. The integrated current on the target is the same in both cases.

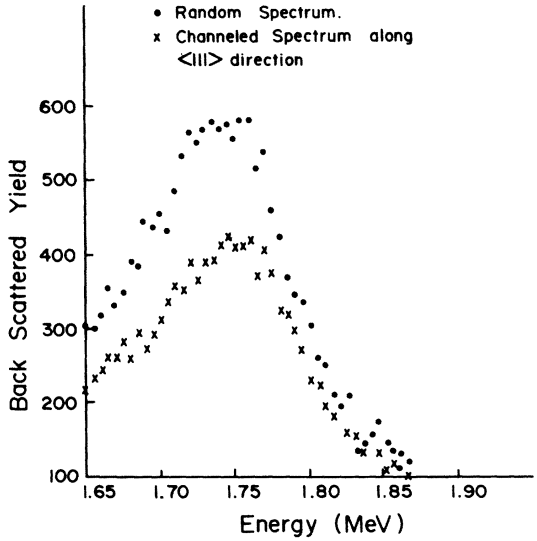

FIG. 8. Energy spectra for 2-MeV α particles backscattered from the ^{153}Eu ions implanted in a Cu single crystal, with the incident beam parallel to the ⟨111⟩ axis and a random direction, respectively. There is a marked reduction in the scattering yield when the beam is aligned along the ⟨111⟩ direction.

along the ⟨110⟩ axis. A similar measurement has been carried out with the incident α beam parallel to the ⟨111⟩ and random directions, respectively. The analysis of the scattered α-particle energy spectra (Fig. 8) has revealed a 65% reduction in the scattering yield in this case showing that about 60% of the impurity atoms are located along the ⟨111⟩ direction, but their absence along the ⟨110⟩ axis clearly indicates that they occupy nonsubstitutional sites. In arriving at these results we have used the relation,

$$\text{substitutional fraction} = \frac{(1-\chi_{\min})_{\text{impurity}}}{(1-\chi_{\min})_{\text{host}}} .$$

III. DISCUSSION AND CONCLUSIONS

The result of the differential PAC measurement on the 1278–123-keV cascade in ^{154}Gd for the implanted sample as given in Fig. 4 shows a typical static-electric quadrupole-interaction behavior.[10] The angular frequency ω_0 in this interaction, equivalent to the smallest nonvanishing energy difference, can be determined from the measured integral attenuation coefficient $\bar{G}_{22}(\infty)$ (Table I), using the expression

$$\bar{G}_{kk}(\infty) = \sum_n S_{kn} \{1/[1+(n\omega_0\tau)^2]\}$$

for an axially symmetric static electric field gradient ($\eta = 0$). In this expression S_{kn} are the geometric coefficients and τ is the mean lifetime of the excited state under consideration (123-keV first 2^+ excited state in ^{154}GD). The assumption of axial symmetry may be justified, since for spin $I = 2$ the effect of η dependence in polycrystalline materials is small.[2] It may be noted that if the field gradients are produced by lattice damage, the assumption of axial symmetry may not hold. However, it has been shown[10] that the change in ω_0 value obtained from $\bar{G}_{22}(\infty)$ is not very sensitive to variation in η (in the region of our interest it is $< 5\%$). The value of ω_0 so obtained ($\omega_0 = 0.298 \times 10^9$ rad/sec) is used to find the times t_1 and t_2 at which the first minimum and second maximum occur in the theoretical $G_{22}(t)$ vs $\omega_0 t/\pi$ plot. Such calculations for different values of the asymmetry parameter η for polycrystalline materials have been carried out in a rather general way by Matthias *et al.*[11] The calculated values agree very well with the experimentally observed ones (Table II) as seen in Fig. 4. It should be pointed out that t_1 and t_2 are not very sensitive to the value of η. While in the present case best agreement with the theoretical calculations is obtained assuming $\eta = 1$, we may also mention that it is realistic to include the variation of electric field gradient from nucleus to nucleus. Such a variation gives rise to distribution in the quadrupole interaction frequency ω_Q. We cannot quantitatively comment on this distribution from the present work since the behavior of $G_{22}(t)$ beyond t_2 could not be ascertained due to the short lifetime ($\tau_{1/2} = 1.17$ nsec) of the 123-keV excited state in ^{154}Gd.

A similar type of behavior of the time-differential perturbation factors (Fig. 4) has also been predicted in a static random magnetic interaction.[12] However in this case the calculated[12] values of t_1 and t_2 are found to be much longer, 3.2 and 5.3 nsec, respectively, as compared to the observed ones (Table II).

The possibility of a predominant static-electric quadrupole interaction in the present case is also indicated from the measured $\bar{G}_{44}(\infty)$ value in the study of the directional distribution of 876–123-keV cascade. It is seen that for the 123-keV state in ^{154}Gd the $\bar{G}_{22}(\infty) < \bar{G}_{44}(\infty)$ (Table I) which is possible only in the case of a static quadrupole interaction.[13] Similar interaction is seen by Ryge *et al.*[7] in their studies of Coulomb excitation recoil implantation of ^{156}Gd and ^{158}Gd, respectively, in Cu backing. Such an interaction in a cubic host like diamagnetic copper is probable, provided the impurity atoms are occupying mostly nonsubstitutional sites and there is considerable damage to the lattice.

The channeling measurements on the Cu single crystals implanted with ^{153}Eu as discussed above have actually shown that more than 90% of impurity ions are located nonsubstitutionally (Sec. IID). Lattice damage is produced while implanting and also while irradiating with neutrons. In this way the existence of a large electric field gradient is possible in a cubic host like Cu.

It is further seen that cooling the implanted sample to 80 °K does not produce any significant change in the attenuation factor (Table I). Such a result is expected since Gd^{3+} ions are in the S state ($L = 0$) and spin-lattice interactions is negligible.

The magnitude of the average electric field gradient in the present case has been calculated using the quadrupole moment $Q_0 = 1.53$ b of the 123-keV state in ^{154}Gd as obtained from experimental $B(E2)$ values[14] and the rotational model.[15] The quadrupole frequency is given by[10]

$$\omega_Q = -\frac{eQV_{zz}}{4I(2I-1)\hbar} \quad \text{for } \eta = 0.$$

TABLE II. Times t_1 and t_2 from the plot of $G_{22}(t)$ vs t. The theoretical values are obtained from Ref. 9.

	Theoretical (nsec)	Experimental (nsec)
t_1	2.53	2.1
t_2	4.53	3.95

In terms of ω_0 for $I=2$, $\omega_Q=\omega_0/3$. The electric field gradient is thus obtained as 3.2×10^{17} volts/cm^2. This should be considered as only an order-of-magnitude calculation because of the assumptions of axial symmetry and nonvariation of the electric field gradient from nucleus to nucleus.

There does not seem to be any magnetic interaction in the present case. We have already mentioned above that the contribution to the magnetic hyperfine interaction in Gd^{3+} ions may arise due to polarization effects. The fields due to core polarization and conduction-electron polarization due to its own $4f$ electrons are approximately equal but opposite in sign[16] and thus may neutralize each other. In the absence of any magnetic interaction the polarization effects caused by neighboring ions also seem to be negligible.

Annealing the implanted sample at 325 °C and also at 500 °C has not shown any change in the attenuation factors. The attenuation factors should increase if internal oxidation takes place as reported in Ref. 8. We have shown that the $\overline{G}_{22}(\infty)$ in an oxide sample (Eu_2O_3) is 0.77 ± 0.06 which is much larger than that observed in the annealed implanted samples (Fig. 5). The absence of any change in the correlation after annealing at different temperatures for different times clearly shows that there is no internal oxidation. We may try to explain this result in two ways. Firstly, findings of Cohen *et al.*[8] are for 50-keV Gd ions implanted in an Fe host. In the present case Eu is implanted into copper at an ion energy of 400 keV. At low implantation energies, some of the oxygen atoms from the surface oxide layer, which get implanted into Fe due to the impact of incident Gd ions, are almost in the same region as the implanted Gd ions (~130 Å). Hence oxidation on annealing might be possible as has been mentioned by Cohen *et al.*[8] When the incident-ion energy is large (400 keV) the oxygen ions will travel a larger distance (~ 900 Å) as compared to the Gd-impurity ions (~500 Å). This may be one of the reasons for not observing internal oxidation in the present case. However, this seems to be rather improbable as there may be considerable distribution in the range of oxygen ions due to the variation in recoil energy depending on scattering angle. The other possibility is that for low-energy implantation the impurity ions are very near the surface and at the time of annealing may get oxidized with the oxygen near the surface, giving rise to the disappearance of hyperfine field at impurity sites because of cubic symmetry following oxidation. Such a thing does not seem to be probable at high-energy implantation where the impurity ions go much deeper into the host material and thus any mixing with the oxide layer on annealing is not possible. The absence of internal oxidation for higher implantation energies is also confirmed by the recent findings of Thome *et al.*[17] in their study of Yb-implanted iron samples.

ACKNOWLEDGMENTS

The authors are very grateful to the Accelerator group of the Institute of Physics, University of Aarhus, Denmark for preparing implanted samples. Thanks are due to S. Panchapakesan and S. D. Shirvalkar for their help during the course of experiments. The co-operation of the Van de Graaff operation staff at BARC, Trombay, is gratefully acknowledged.

[1] L. Grodzins, Annu. Rev. Nucl. Sci. 18, 291 (1968).
[2] B. Herskind, in *Hyperfine Interactions in Excited Nuclei*, edited by G. Goldring and R. Kalish (Gordon and Breach, New York, 1971), p. 987.
[3] R. R. Borchers, in Ref. 2, p. 31.
[4] B. I. Deutch and G. M. Heestand, in *Angular Correlation in Nuclear Disintegration*, edited by H. Van Krugten and B. Van Nooijen (Rotterdam U. P., Netherlands, 1971), p. 487.
[5] B. I. Deutch, K. Bonde Nielsen, and H. Bernas, Phys. Lett. B 27, 209 (1968).
[6] J. C. Weddington, K. A. Hagemann, S. Ogaza, D. Kiss, B. Herskind, and B. I. Deutch, in *Nuclear Reactions Induced by Heavy Ions*, edited by R. Bock and W. R. Hering (North-Holland, Amsterdam, 1970), p. 438.
[7] P. Ryge, H. W. Kugel, and R. R. Borchers, in Ref. 2, p. 1043.
[8] R. L. Cohen, G. Beyer, and B. I. Deutch, Phys. Rev. Lett. 33, 518 (1974).
[9] L. Varnell, J. D. Bowman, and J. Trischuk, Nucl. Phys. A 127, 270 (1969).
[10] H. Frauenfelder and R. M. Steffen, in *Alpha, Beta, and Gamma Ray Spectroscopy*, edited by K. Siegbahn (North-Holland, Amsterdam, 1965), p. 1118.
[11] E. Matthias, W. Schneider, and R. M. Steffen, Phys. Lett. 4, 41 (1963); also Ark. Fys. 24, 97 (1963).
[12] E. Matthias, S. S. Rosenblum, and D. A. Shirley, Phys. Rev. Lett. 14, 46 (1965).
[13] A. Abragam and R. V. Pound, Phys. Rev. 89, 1306 (1953).
[14] B. Elbek, M. C. Ølesen, and O. Skilbried, Nucl. Phys. 19, 523 (1960).
[15] K. Alder, A. Bohr, T. Huus, B. R. Mottelson, and A. Winther, Rev. Mod. Phys. 28, 432 (1956).
[16] S. Hufner and J. H.Wernick, in *Hyperfine Structure and Nuclear Radiations*, edited by E. Matthias and D. A. Shirley (North-Holland, Amsterdam, 1968), p. 463.
[17] L. Thome, H. Bernas, J. Chaumont, F. Abel, M. Bruneaux, and C. Cohen, Phys. Lett. A 54, 37 (1975).